Reply to Reviewer #1 Comments

General comment

Present work is a case study of a possible interaction of atmospheric gravity waves (GWs) and equatorial plasma bubbles (EPBs). The authors observed South to North propagation of GWs, when an EPB was drifting eastward. After the interaction, the EPB (DP1) revived, extending its latitudinal extension and the 6300 depletion became much stronger. The authors tried to explain the observational evidence as an interaction of E-field generated by GWs and EPB. They concluded that "fossil depletion" DP1 revived and became an "active depletion" under the passage of GWs." The interpretation and argument are interesting and worth to pointing and to discuss, since such observational reports are still limited in the literature.

Reply: We sincerely thank the esteemed Reviewer for his tremendous encouragement and invaluable insight into our submission. His critical comments have provided us with insightful perspectives to enhance the clarity and robustness of our findings. We have tried our level best to address his concerns in this Revised Version.

However, I feel a serious concern in the airglow images and the image data analysis. Regarding the signature of thermospheric gravity waves (f1, f2), the authors mentioned that the wave crests can be seen clearly in Figure 1 and Figure 3(c,d). To my seeing, it is very difficult to recognize the wave fronts f1 and f2 from Figure 1 and 3(c, d). Since the wave fronts in question are located close to the image horizon, it is further difficult to resolve horizontal structure. The authors should explain how they transferred the images in geographic coordinates and calculate the wave characteristics. If it is not the case, how the linear coordinates are decided. Besides it, the optical filter for 6300 imaging normally includes OH emissions, of which intensity is much stronger near the horizon, say 75 to 80 degree of zenith angle. How the authors could eliminate the OH contamination. The authors can explain those mattes in the section of Instrumentation and data analysis procedure.

Reply: Sincere thanks for these critical comments and suggestions which indeed helped us to improve the presentation of our results.

1. We agree with Reviewer that the signatures of thermospheric gravity waves are not clear and very faint. Under these situations, time-difference (TD) images have proven ability to reflect the faint GWs activity. We generated such TD images and present below some of them during 1742-1830 UT that do show faint fronts of GWs. We present labelled and unlabelled sequence of OI 630 nm images, respectively, on the left and right for the kind preview of Reviewer.

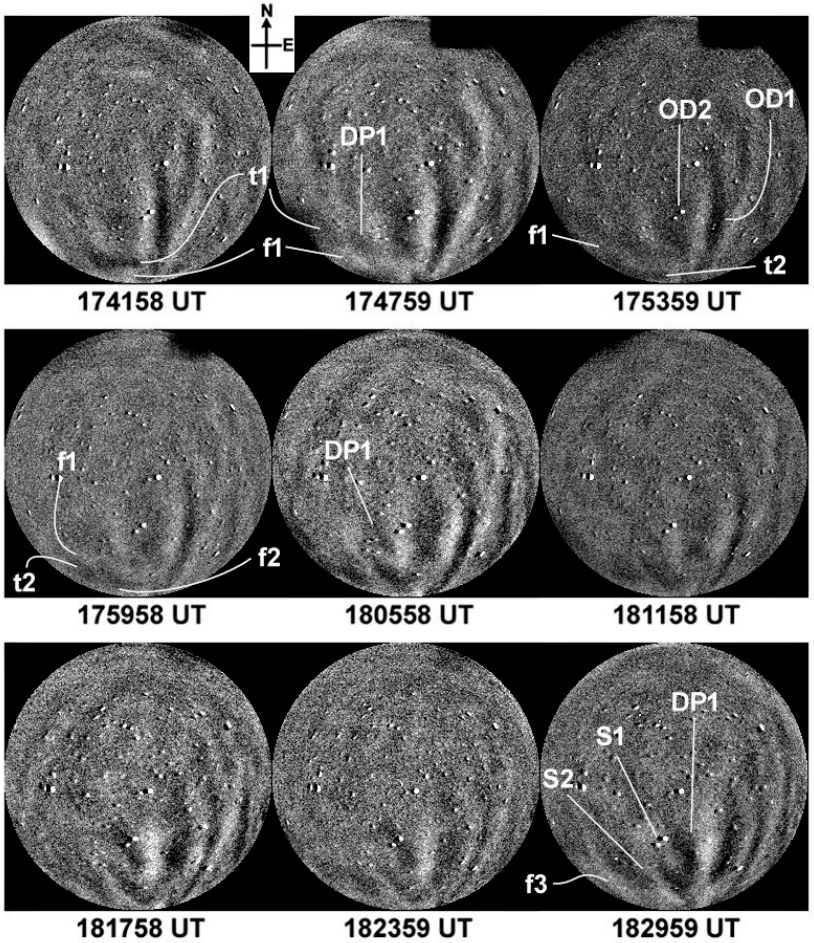

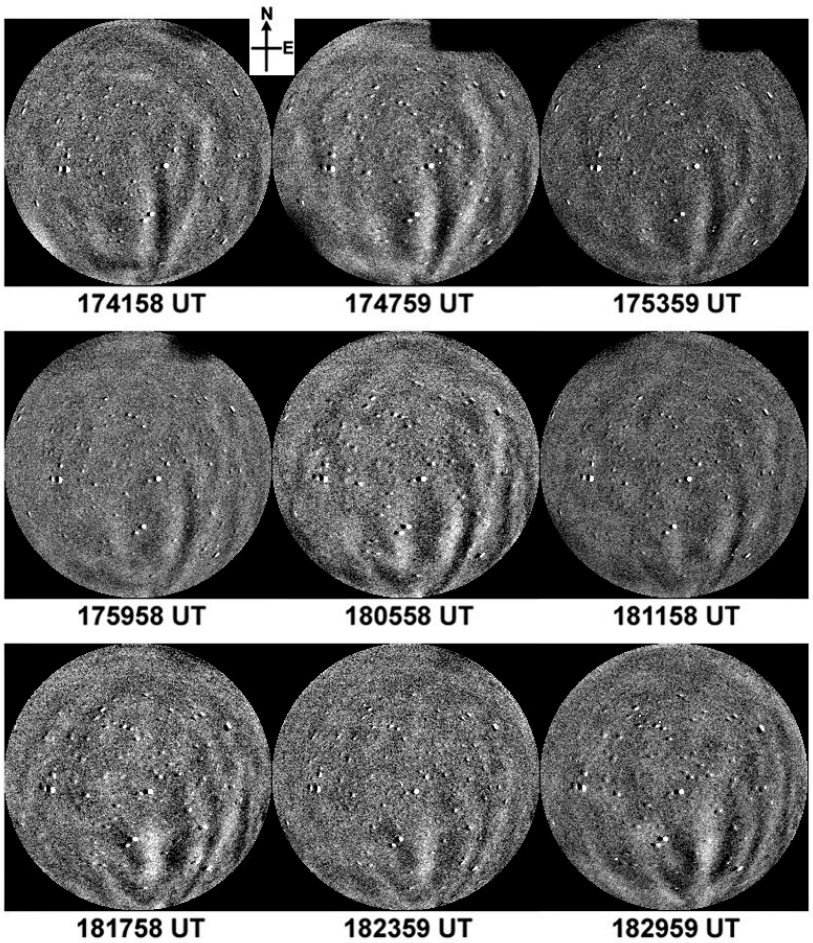

2. As suggested, we have Re-written the **Introduction and data** section as under as:

Under the ***CAWSES India Phase II Programme***, an ASAI was installed for limited nightglow observations at Ranchi (23.3º N, 85.3º E, mlat. ~19º N), located near the crest of equatorial ionization anomaly (EIA) in India during April 2012. Parihar et al. (2017) and Parihar (2019) have described this ASAI system in detail. OI 630 nm emission was monitored using a 2.2 nm half-power bandwidth optical filter having transmittance of ~77%. Our imager's field-of-view roughly covered about 7-8° latitude/longitude region at 250 km over Ranchi. Airglow images were flat-fielded to reduce the inhomogeneous contribution at lower elevations due to van Rhijn effect and non-uniform sensitivity of CCD detector at different pixels. Next, following the technique described by Wrasse et al. (2021), we detrended the individual images to enhance the contrast of airglow features using an hour running average image. Using known astral positions and assuming OI 630 nm emission peak at 250 km, the geographic coordinates of each pixel was determined following the technique of Garcia et al. (1997). Using this information, all-sky images were unwarped. We follow the technique discussed by Pimenta et al. (2003) to determine the drift velocity of depletions. First, for a given latitude, two intensity profiles along east-west direction as a function of distance was generated using two successive unwarped images. Next, the east-west displacement of depletion was estimated using these two profiles from which drift speed was determined (see Pimenta et al., 2003 for details of this technique). Similarly, the propagation characteristics of GW fronts were estimated by tracking faint crest and trough along the propagation direction in the consecutive images. As GW fronts were unclear in images, we used contrast-enhanced images. We, also, generated NS keograms to visualize GW traces and determine their speed. A keogram is a time-versus-latitude plot generated by extracting a NS column from individual images and stacking them horizontally. Next, GWs speed was, also, estimated from the slope of wave traces seen in these keograms (Makela et al., 2006). We looked into the total electron content (TEC) measurements from an *International GNSS Service* station Hyderabad (17.3° N, 78.6° E, mlat. ~12.0° N, located nearby and south of Ranchi) to ascertain GW activity seen in the ASAI observations (Source: https://t-ict4d.ictp.it/nequick2/gnss-tec-calibration, Ciraolo et al., 2007). Quiet geomagnetic conditions prevailed on this night with $Kp < 2$, $Ap = 4$, and $-4 < Dst < 10$ *nT*.

3. We describe in brief the technique used by Pimenta et al. (2003) to estimate the drift velocity of depletions and GWs.

Using known astral positions and assuming OI 630 nm emission peak at 250 km, the geographic coordinates of each pixel was determined following the technique of Garcia et al. (1997). Using this information, all-sky images were unwarped. We follow the technique discussed by Pimenta et al. (2003) to determine the drift velocity of depletions. First, for a given latitude, two intensity profiles along east-west direction as a function of distance was generated using two successive unwarped images. Next, the east-west displacement of depletion was estimated using these two profiles from which drift speed was determined (see Pimenta et al., 2003 for details of this technique). Similarly, the propagation characteristics of GW fronts were estimated by tracking faint crest and trough along the propagation direction in the consecutive images. As GW fronts were unclear in images, we used contrast-enhanced images. We, also, generated NS keograms to visualize GW traces and determine their speed.

A typical unwarped image at 192358 UT in presented below:

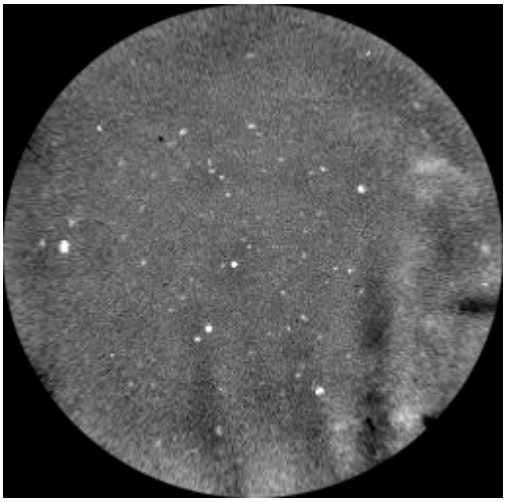

4. We agree with Reviewer that OH emissions can contaminate OI 630 nm nightglow. We used a 2.2 nm narrow half-power bandwidth optical filter to monitor OI 630 nm emission which can be contaminated by P_2 line of OH (9, 3) Meinel band at 629.8 nm. As a cross-check, we looked into OH broadband emission which indicated no GW activity at the MLT region. A typical OH broadband image is presented below:

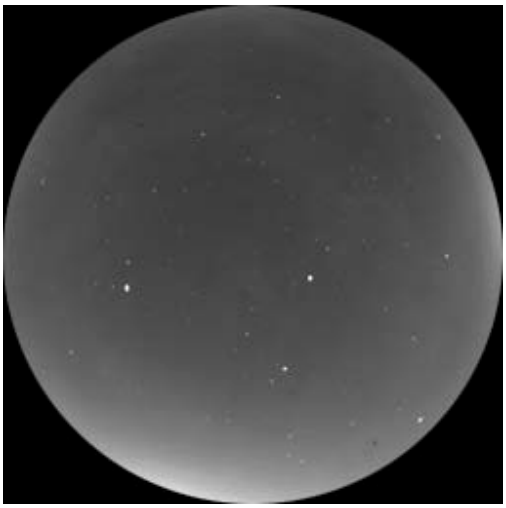

We, further, looked into TEC measurements from an IGS station Hyderabad (located nearby and south of Ranchi) which do show the presence of wave like variations. As such, we believe that GW fronts seen in OI 630 nm are the signatures of thermospheric GW activity.

In conclusion, the present manuscript would be necessary to improve data analysis method and to convince readers to see the clear signature of wave structure of GWs in the 6300 emission layer.

Reply: We sincerely thank Reviewer for this critical comment. We have tried to bring out clarity in Presentation and Figures to show the signatures of GWs in OI 630 nm images.

Individual comments are below:

Line 133 (filter characteristics of 6300 imaging): please include the filter characteristics (HPBW, for example).

Reply: Many thanks. We have added this information.

Correction: OI 630 nm emission was monitored using a 2.2 nm half-power bandwidth optical filter having transmittance of ~77%.

Line 144 (keogram): please mention how to produce the keogram and how to calculate the wave characteristics from the keogram. What is the latitudinal extension (in km) of the keogram Figure 3 (a, b) ?

Reply: Many thanks. We have added the following text in this Revised version.

Correction 1: A keogram is a time-versus-latitude plot generated by extracting a NS column from individual images and stacking them horizontally. Next, GWs speed was, also, estimated from the slope of wave traces seen in these keograms (Makela et al., 2006).

Correction 2: We have corrected the Figure for latitudinal extension as under as:

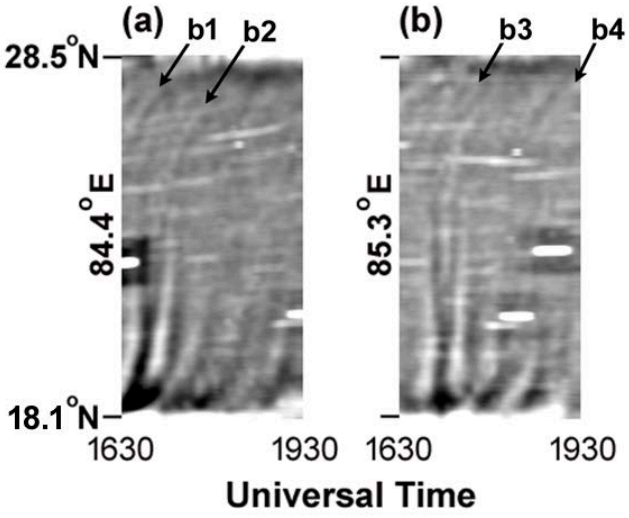

Line 161 (keogram): Are these keograms made by using original images or geographically coordinated (unwarped) images ? Please make indication by arrow the GW signature in the Figures 3 (a) and (b).

Reply: Many thanks. We have generated keograms from flat-fielded and contrast enhanced images. Used images were not geographically corrected ones. We have considered a NS column of individual images corresponding to desired longitude as depicted below and stacked them horizontally.

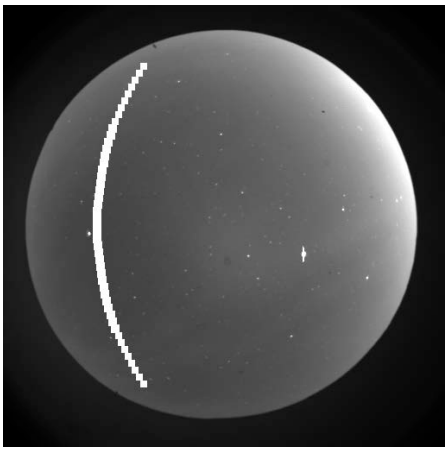

We have, also, marked the GW traces by black arrow ‘b1’, ‘b2’, ‘b3’ and ‘b4’ used for determining their phase speed as suggested.

Lines 166-167 (Being faint in nature, GWs signatures in ASAI images were getting lost in the geographic unwarping process): As the authors mentioned, it is difficult to estimate wave characteristics from the wave crests located at a large zenith angle. It means that there is a large uncertainty to get the wave characteristics from the wave fronts located in the corner of an all sky image. If the wave fronts (f1 and f2) are located at around 75 to 80 degrees of zenith angle, for example, one degree of distance corresponds to longer than 40-50 km at 250 km of altitude. The authors should keep in mind such uncertainty in their calculation of wave characteristics.

Reply: We agree with Reviewer and sincerely thank for this critical comment. We have considered the wave fronts and troughs located within 65 degrees of zenith angle. GW front ‘f1’ and trough preceding it were located within this range around 1800 UT. We have, also, relied on the wave traces seen over the North in NS keograms.

Line 169 (intensity profiling technique): Please explain the technique,

Reply: Many thanks. We have added the following text in “**Instrumentation and data**” Section: **Correction:** We follow the technique discussed by Pimenta et al. (2003) to determine the drift velocity of depletions. First, for a given latitude, two intensity profiles along east-west direction as a function of distance was generated using two successive unwarped images. Next, the east-west displacement of depletion was estimated using these two profiles from which drift speed was determined (see Pimenta et al., 2003 for details of this technique). Similarly, the propagation characteristics of GW fronts were estimated by tracking faint crest and trough along the propagation direction in the consecutive images.

Line 170 (wave characteristics and Figure 3): The authors used keogramas (Figs 3(a,b) to calculate the wave characteristics. Please show explicitly the wave traces used in the figure. The authors pointed the wave signatures in the south edge of the image, However, the keograms show GW trace in the northern part. No propagating signature in the southern part. Please explain N-S scale of the keogram and put arrow signs to show the GW traces.

Reply: We sincerely thank with Reviewer and agree that wave traces were seen over North. Because of the co-existence of GW fronts and depletions together and their interaction over the South, we were unable to see such traces. As suggested, we have corrected the keograms as under as:

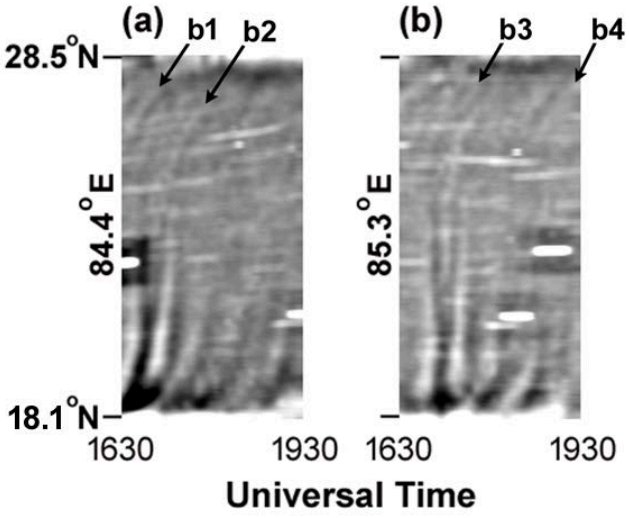

Line 176 (G27): Where is G27 ? Please point it.

Reply: Many thanks for pointing out this shortcoming in our presentation. We have limited the scatter plot to a few IPP trajectories and corrected Figure is as under as:

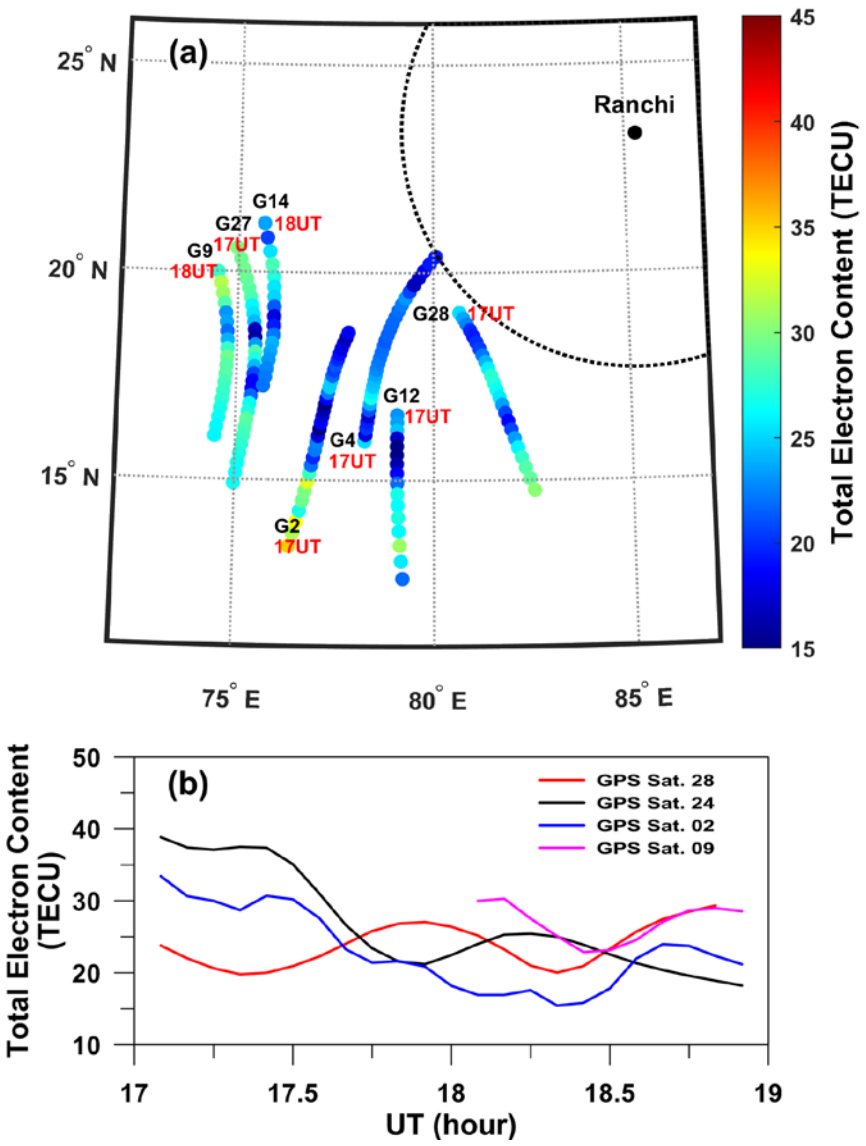

Line 180 (wave characteristics): please explain how the authors obtained this characteristic. Please remember that an IPP trajectory has two variables, time and space. Figure 3(f), therefore, shows TEC variation as a function of time and coordinates.

Reply: We sincerely thank Reviewer for bringing out this shortcoming in our presentation. We have corrected the text as under as:

Correction:

Of our interest is G28's TEC measurement as its IPPs trajectory lay close to the imager's ROI1 during 1700-1800 UT which showed a strong signature of GWs. By performing the periodogram

analysis of the temporal and spatial variation of its TEC, we estimated the propagation characteristics of GW to be τ ~0.95 ± 0.03 h, λ ~229 ± 12 km, and υ ~67 ± 5 m/s, and is in good agreement with the ASAI observations. Further, the propagation direction of GWs seen in airglow imaging is in good agreement with these previous reports.

Lines 198-204 and Figure 1: The authors tried to show the interaction of DP1 and GW f1 and f2, using Figure 1. However, it is hard to see such spatial and temporal variations of DP1, f1 and f2, those pointed by the authors. If the authors believe that the process was really happening, they must show airglow images with much clear way, perhaps increasing image contrast by subtracting one image from the other as shown in Figure 3(c,d).

Reply: We sincerely thank Reviewer for bringing out this shortcoming in our presentation. We have corrected **Figure 1** as:

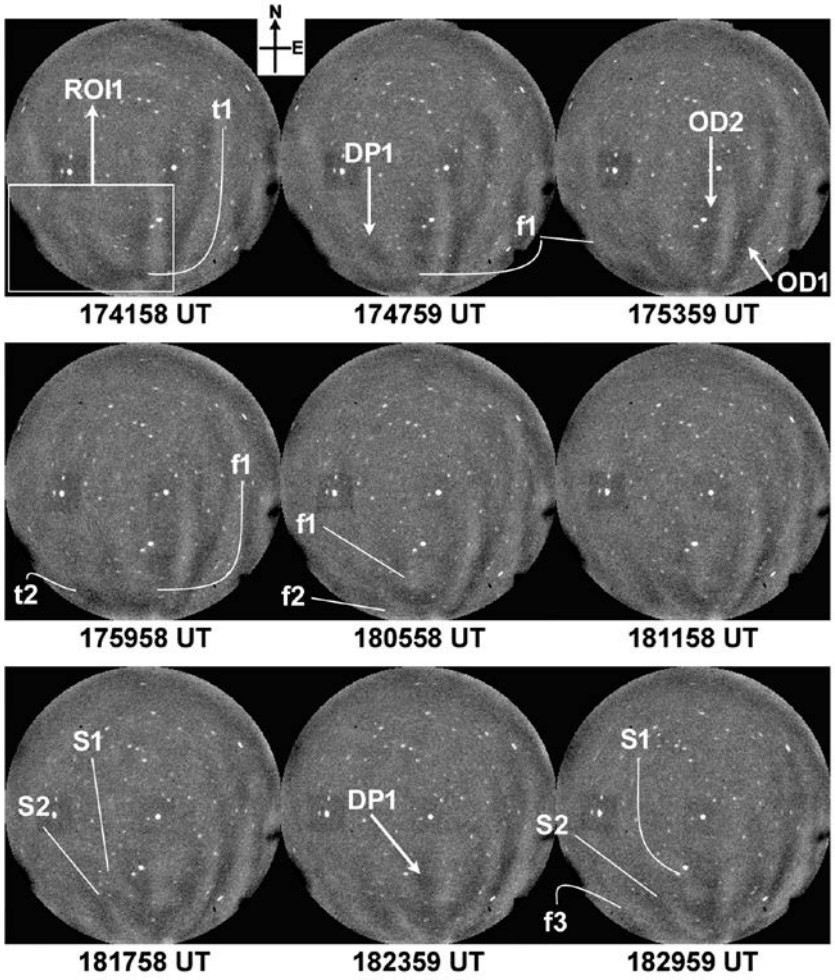

Corrected Figure 2:

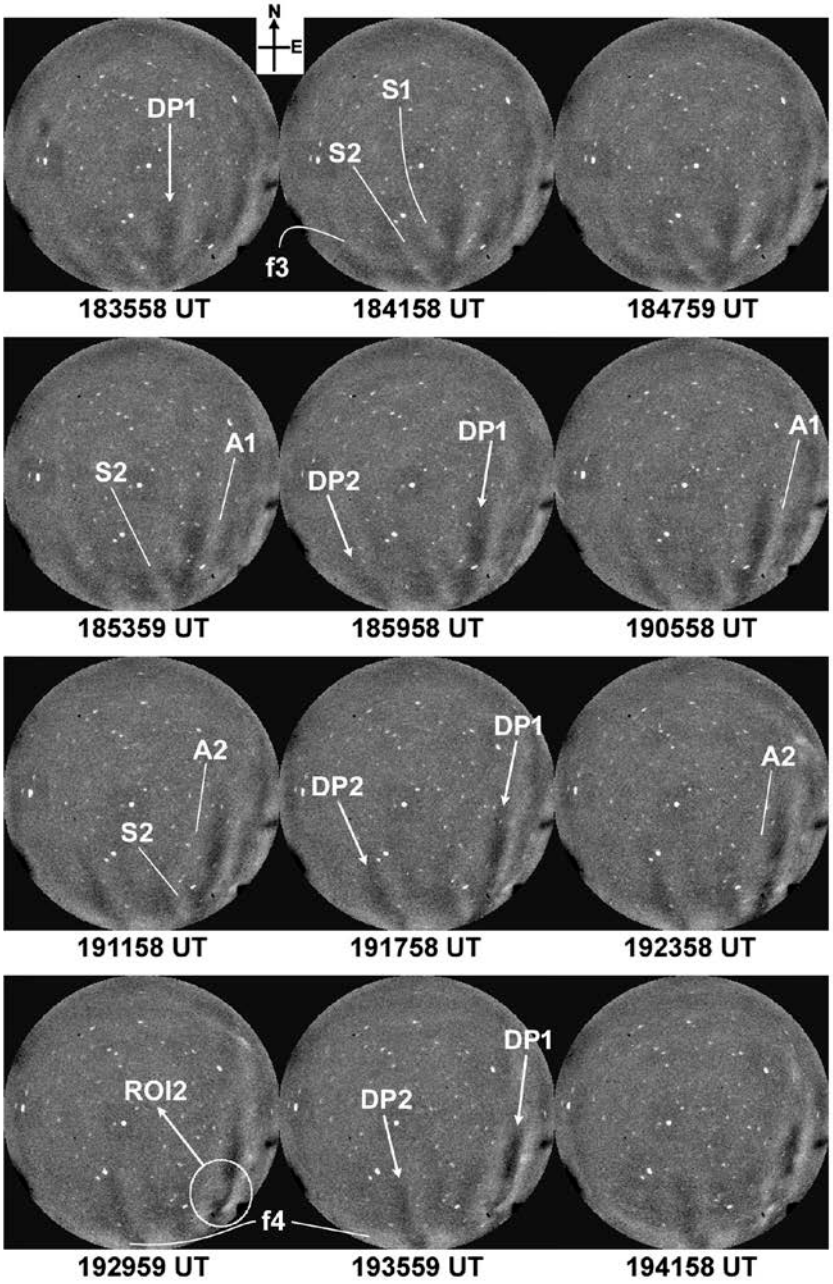

Lines 241-243 (GWs deform ,,,, act as a seed to GRT instability): please put references on it.

Reply: Many thanks. We have included References as under as:

Correction: GWs are well known to deform the bottom side plasma of the F-region into the wavelike ionization structures that then act as a seed to GRT instability, which, in turn, generates irregularities (Kelley et al., 1981; Hysell et al., 1990; Huba and Liu, 2020).